

Non-collinearity in di-jet fragmentation in electron-positron scattering

P.J. Mulders^{1,2} and C. Van Hulse^{3,4,*}

¹Theory Group, Nikhef, 1098 XG Amsterdam, the Netherlands

²Department of Physics and Astronomy, Faculty of Science, VU, 1081 HV Amsterdam, the Netherlands

³Department of Theoretical Physics and History of Science,

University of the Basque Country UPV/EHU, 48080 Bilbao, Spain

⁴School of Physics, University College Dublin, Dublin 4, Ireland

We study fragmentation in electron-positron annihilation assuming a di-jet situation, using variables defined independent of any frame. In a collinear situation some of the variables are centered around zero with the small deviations attributed to intrinsic transverse momenta and large deviations attributed to additional hard subprocesses. Of course there is a gradual transition. Our modest goal is to show that covariantly defined variables are well suited to get a feeling for the magnitude of intrinsic transverse momenta.

PACS numbers: 11.30.Cp, 12.15.-y, 12.38.Aw

I. INTRODUCTION

Inclusive production of two hadrons in electron-positron annihilation is a way to study intrinsic transverse momenta in the fragmentation functions of those hadrons. The non-collinearity in the process can be defined as a spacelike vector q_T to be specified below. In the basic transverse momentum dependent (TMD) treatment, the q_T dependence is a folding of intrinsic transverse momenta of the two fragmentation functions in the case of inclusive two-hadron production. Of course, we have in mind the situation shown in figure 1 where the two hadrons emerge in two jets with opposite momenta, where in zeroth order the jet directions can be identified with the parent partons. In this note, we just want to look at how scaling variables constructed with invariants in the scattering process can be linked to the hadron momentum fractions in a di-jet situation. One has to keep in mind that partonic transverse momenta are not unique as they depend on a Sudakov expansion for the momenta involving a light-like vector n ($n^2 = 0$) conjugate to the hadron momentum $P \cdot n = 0$. The light-like vector ac-

quires a meaning if in a hard process transverse momenta are probed and it then depends on a combination of hard momenta in the scattering process. This is relevant for mass corrections (from hadron masses) and factorisation. In this note, we are just after observables that like rapidity or pseudo-rapidity are useful as measures of non-collinearity and intrinsic transverse momenta.

II. BASIC DEFINITIONS

We look at $e^-(l_1) + e^+(l_2) \rightarrow H_1(P_1) + H_2(P_2) + \text{anything}$, having in mind an intermediate step into two partons $e^-(l_1) + e^+(l_2) \rightarrow \text{parton}_1(k_1) + \text{parton}_2(k_2)$. The di-jet situation is then the case that $k_1^2 = k_2^2 = 0$. The measure for non-collinearity [1–4] is given by

$$q_T \equiv q - \frac{P_1}{\zeta_1} - \frac{P_2}{\zeta_2}, \quad (1)$$

with $q = l_1 + l_2 = k_1 + k_2$ and the requirements that $P_1 \cdot q_T = P_2 \cdot q_T = 0$ implying that the hadrons determine the light-like directions in which case the transverse directions for two-particle inclusive (2PI) annihilation are given by $g_T^{\mu\nu} = g^{\mu\nu} - P_1^{\{\mu} P_2^{\nu\}} / 2P_1 \cdot P_2$. This is sufficient to solve for what we will refer to as 2PI momentum fractions $\zeta_{1,2}$, which do include mass corrections,

$$\zeta_1 = \frac{P_1 \cdot P_2 - \frac{M_1^2 M_2^2}{P_1 \cdot P_2}}{P_2 \cdot q - \frac{M_2^2 P_1 \cdot q}{P_1 \cdot P_2}}, \quad (2)$$

and

$$\zeta_2 = \frac{P_1 \cdot P_2 - \frac{M_1^2 M_2^2}{P_1 \cdot P_2}}{P_1 \cdot q - \frac{M_1^2 P_2 \cdot q}{P_1 \cdot P_2}}, \quad (3)$$

with M_i representing the hadron masses.

The (negative) invariant length of q_T^2 signalling non-

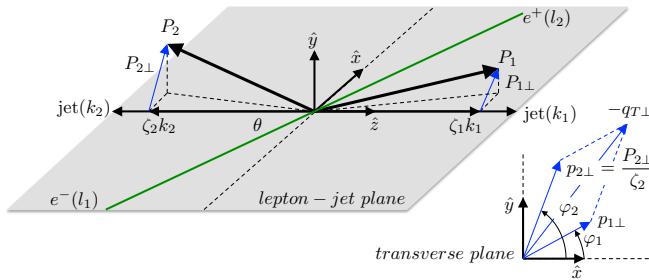


FIG. 1: Basic vectors in $e^- e^+$ annihilation (momenta l_1 and l_2) into two hadrons with momenta P_1 and P_2 originating from two (non-observed) partons with momenta k_1 and k_2 .

*Electronic address: p.j.g.mulders@vu.nl, cvanhuls@mail.cern.ch

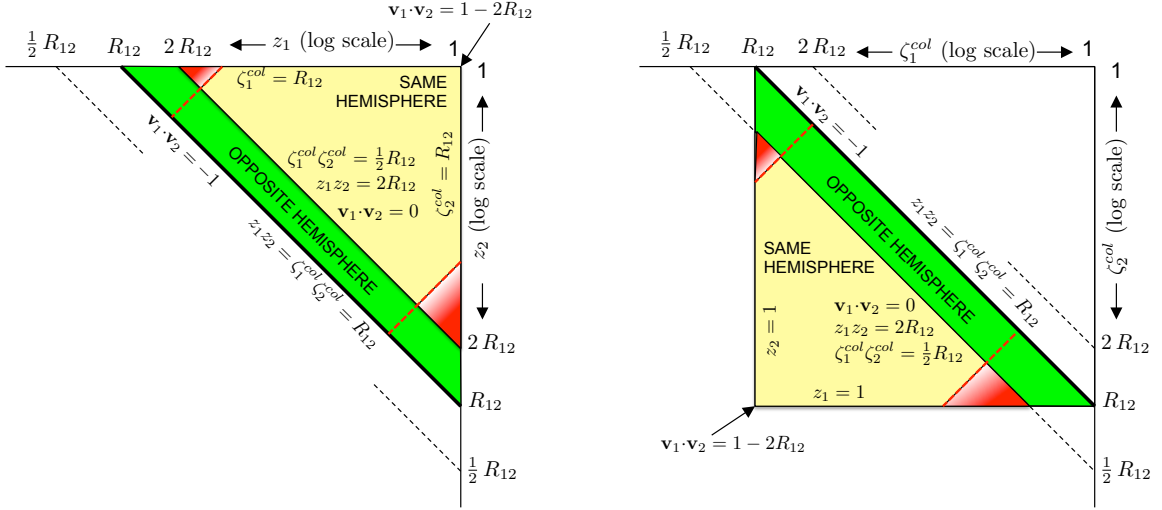


FIG. 2: Range of z_i and ζ_i^{col} for a given value of the ratio $R_{12} = 2 P_1 \cdot P_2 / s$, divided in opposite and same hemisphere events according to Eq. 11. An indication of the regions where (for sufficiently small R_{12}) the quantities ζ_i turn negative is indicated as the red triangular regions (see discussion following Eq. 14). The distance of points to the line $z_1 z_2 = \zeta_1^{col} \zeta_2^{col} = R_{12}$ is a measure of q_T^2 / s (see Eqs. 6 and 16).

collinearity can be expressed in the invariants as

$$q_T^2 = q^2 \left(1 - \frac{P_1 \cdot q}{\zeta_1 q^2} - \frac{P_2 \cdot q}{\zeta_2 q^2} \right) \quad (4)$$

$$= q^2 \left(1 - \frac{2P_1 \cdot P_2}{\zeta_1 \zeta_2 q^2} - \frac{M_1^2}{\zeta_1^2 q^2} - \frac{M_2^2}{\zeta_2^2 q^2} \right) \quad (5)$$

$$= \frac{q^2}{2} \left(2 - \frac{z_1}{\zeta_1} - \frac{z_2}{\zeta_2} \right), \quad (6)$$

where z_1 and z_2 are the equivalents of the Bjorken scaling variable in deep-inelastic scattering [5],

$$z_1 = \frac{2P_1 \cdot q}{q^2} \quad \text{and} \quad z_2 = \frac{2P_2 \cdot q}{q^2}. \quad (7)$$

In the e^-e^+ center-of-mass frame, henceforth called CM frame, these are $z_i = 2E_i / \sqrt{s}$, where $s = 2l_1 \cdot l_2$. In the 2PI case, these variables are restricted to $0 \leq z_i \leq 1$ [5]. The 2PI variables ζ_1 and ζ_2 are not constrained to this interval, as will be illustrated further.

The variables z_i together with the ratio

$$R_{12} = \frac{2 P_1 \cdot P_2}{q^2} = \frac{2 P_1 \cdot P_2}{s} \quad (8)$$

can help to identify hadrons that fit a description as belonging to opposite or same parton jets. We note first of all that this ratio satisfies $R_{12} < 1$, with the upper limit, up to mass corrections, reached in an elastic process like $e^+e^- \rightarrow \pi^+\pi^-$. An appropriate lower limit for our considerations would be something like back-to-back pions with a minimal energy E of around 0.5 GeV in the CM frame, corresponding to $R_{12} \gtrsim (1 \text{ GeV}^2) / s$. In the CM frame the following ratio holds for any pair,

$$\frac{4 P_1 \cdot P_2}{z_1 z_2 s} = \frac{E_1 E_2 - \mathbf{P}_1 \cdot \mathbf{P}_2}{E_1 E_2} = 1 - \mathbf{v}_1 \cdot \mathbf{v}_2, \quad (9)$$

thus

$$z_1 z_2 = \frac{2 R_{12}}{1 - \mathbf{v}_1 \cdot \mathbf{v}_2}, \quad (10)$$

where the three-momentum scalar product $\mathbf{v}_1 \cdot \mathbf{v}_2$, here and in the following evaluated in the CM frame, is positive for fast hadrons within a cone around the same fragmenting parton, while it is negative for fast hadrons from different parton jets, as indicated in figure 1. The limit between both situations, with two fast hadrons perpendicular to each other, corresponds to $z_1 z_2 = 2 R_{12}$, resulting in the criterion

$$\begin{aligned} \text{opposite hemisphere: } & R_{12} \leq z_1 z_2 \leq 2 R_{12}, \\ \text{same hemisphere: } & 2 R_{12} \leq z_1 z_2 \leq 1, \end{aligned} \quad (11)$$

as a first-order requirement to characterise hadrons as belonging to back-to-back parton jets or to the same parton jet, respectively.

We want to further illustrate this by a comparison with the collinear fractions ζ_1^{col} and ζ_2^{col} , scaling variables defined as [6]

$$\zeta_1^{col} = \frac{P_1 \cdot P_2}{P_2 \cdot q} \quad \text{and} \quad \zeta_2^{col} = \frac{P_1 \cdot P_2}{P_1 \cdot q}. \quad (12)$$

These variables are also limited to $0 \leq \zeta_i^{col} \leq 1$ [5]. We note that

$$z_1 \zeta_2^{col} = \zeta_1^{col} z_2 = R_{12}. \quad (13)$$

The range of the scaling variables ζ_i^{col} and z_i is illustrated in figure 2. Using $\epsilon_i = M_i^2 / P_1 \cdot P_2$ we have the exact relations

$$\zeta_1 = \zeta_1^{col} \frac{1 - \epsilon_1 \epsilon_2}{1 - \epsilon_2 \zeta_1^{col} / \zeta_2^{col}}, \quad \zeta_2 = \zeta_2^{col} \frac{1 - \epsilon_1 \epsilon_2}{1 - \epsilon_1 \zeta_2^{col} / \zeta_1^{col}}. \quad (14)$$

From it, we obtain the region where ζ becomes negative, e.g., $\zeta_1 < 0$, when $\zeta_2^{col} < \epsilon_2 \zeta_1^{col} = (2M_2^2/R_{12}s)\zeta_1^{col}$, or $z_2 < (2M_2^2/R_{12}s)z_1$. It just signals that one is outside the region of validity for simple parton branching and fragmentation. Note that the regions for hadrons 1 and 2 may be different (hence the asymmetry of the effect in figure 2). Up to ϵ^2 terms we have (if ζ_2^{col} is not too small)

$$\zeta_1 \approx \zeta_1^{col} (1 + \epsilon_2 \zeta_1^{col} / \zeta_2^{col}), \quad (15)$$

(thus $\zeta_i \gtrsim \zeta_i^{col}$) and for sufficiently small ϵ_i , for instance for pions,

$$\zeta_{1/2} \approx z_{1/2} \left(1 + \frac{q_T^2}{q^2} \right) \quad (16)$$

(thus $\zeta_i < z_i$ for small ϵ_i).

There is a second measure for non-collinearities, which is the determinant of the four measured four-momenta,

$$D_T \equiv -\frac{4\epsilon^{l_1 l_2 P_1 P_2}}{\zeta_1 \zeta_2 s^{3/2}} = -\frac{4\epsilon_{\mu\nu\rho\sigma} l_1^\mu l_2^\nu P_1^\rho P_2^\sigma}{\zeta_1 \zeta_2 s^{3/2}}. \quad (17)$$

Here, a particular normalisation has been chosen, a choice that will become clear in the next section via the link to the intrinsic transverse momentum. The invariant q_T^2 only signals that the lepton momenta and hadron momenta are not in a single plane, while the determinant contains also information on the relative orientations of the hadrons.

III. INTERPRETING NON-COLLINEARITIES

For the interpretation of the non-collinearities defined in the previous section, it is convenient to make the four vectors explicit in the leptonic and partonic restframe, using either $p = (p^0, p^1, p^2, p^3)$ or $p = [p^-, p^+, p_T^1, p_T^2]$ with $p^\pm = (p^0 \pm p^3)/\sqrt{2}$, and starting with

$$l_1 = \frac{\sqrt{s}}{2} \begin{pmatrix} 1 \\ 0 \\ 0 \\ 1 \end{pmatrix} = \sqrt{\frac{s}{2}} \begin{bmatrix} 0 \\ 1 \\ 0 \\ 0 \end{bmatrix}, \quad (18)$$

$$l_2 = \frac{\sqrt{s}}{2} \begin{pmatrix} 1 \\ 0 \\ 0 \\ -1 \end{pmatrix} = \sqrt{\frac{s}{2}} \begin{bmatrix} 1 \\ 0 \\ 0 \\ 0 \end{bmatrix},$$

and the partonic light-like momenta

$$k_1 = \frac{\sqrt{s}}{2} \begin{pmatrix} 1 \\ \sin \theta \\ 0 \\ \cos \theta \end{pmatrix} = \sqrt{\frac{s}{2}} \begin{bmatrix} -t/s \\ -u/s \\ \sqrt{2tu}/s \\ 0 \end{bmatrix},$$

$$k_2 = \frac{\sqrt{s}}{2} \begin{pmatrix} 1 \\ -\sin \theta \\ 0 \\ -\cos \theta \end{pmatrix} = \sqrt{\frac{s}{2}} \begin{bmatrix} -u/s \\ -t/s \\ -\sqrt{2tu}/s \\ 0 \end{bmatrix}. \quad (19)$$

We have used here the Mandelstam variables in the process $e^-e^+ \rightarrow \text{jet}_1 \text{jet}_2$,

$$\begin{aligned} s &= q^2 = 2l_1 \cdot l_2, \\ -t &= 2l_1 \cdot k_1 = s \sin^2 \left(\frac{1}{2}\theta \right) \\ -u &= 2l_1 \cdot k_2 = s \cos^2 \left(\frac{1}{2}\theta \right) \end{aligned} \quad (20)$$

and angle θ for which

$$\cos \theta = \frac{t-u}{s}, \quad \sin \theta = \frac{2\sqrt{tu}}{s}. \quad (21)$$

If we take the jet direction as z-axis, we are in a frame in which the momenta of the hadrons will have perpendicular components indicated as pseudo-quark momenta $p_{i\perp} \equiv P_{i\perp}/\zeta_i$. The hadron momenta can be written as

$$\frac{P_1}{\zeta_1} = \frac{\sqrt{s}}{2} \begin{pmatrix} 1 + \mu_{1\perp}^2/s \\ 2p_{1\perp}^x/\sqrt{s} \\ 2p_{1\perp}^y/\sqrt{s} \\ 1 - \mu_{1\perp}^2/s \end{pmatrix} = \sqrt{\frac{s}{2}} \begin{bmatrix} \mu_{1\perp}^2/s \\ 1 \\ p_{1\perp}^x \sqrt{2/s} \\ p_{1\perp}^y \sqrt{2/s} \end{bmatrix},$$

$$\frac{P_2}{\zeta_2} = \frac{\sqrt{s}}{2} \begin{pmatrix} 1 + \mu_{2\perp}^2/s \\ 2p_{2\perp}^x/\sqrt{s} \\ 2p_{2\perp}^y/\sqrt{s} \\ -1 + \mu_{2\perp}^2/s \end{pmatrix} = \sqrt{\frac{s}{2}} \begin{bmatrix} 1 \\ \mu_{2\perp}^2/s \\ p_{2\perp}^x \sqrt{2/s} \\ p_{2\perp}^y \sqrt{2/s} \end{bmatrix}, \quad (22)$$

where $\mu_{i\perp}^2 \equiv (M_i^2 - P_{i\perp}^2)/\zeta_i^2 = M_i^2/\zeta_i^2 + \mathbf{p}_{i\perp}^2$. These momenta are measurable quantities if the jet axis (e.g. identified with a thrust axis) is known, since the angles assume the lepton-jet plane to be the x-z plane. In this frame the partonic momenta do not have transverse components, thus $k_{i\perp} \equiv 0$. Thus explicitly the partonic momenta are

$$k_1 = \frac{\sqrt{s}}{2} \begin{pmatrix} 1 \\ 0 \\ 0 \\ 1 \end{pmatrix} = \sqrt{\frac{s}{2}} \begin{bmatrix} 0 \\ 1 \\ 0 \\ 0 \end{bmatrix},$$

$$k_2 = \frac{\sqrt{s}}{2} \begin{pmatrix} 1 \\ 0 \\ 0 \\ -1 \end{pmatrix} = \sqrt{\frac{s}{2}} \begin{bmatrix} 1 \\ 0 \\ 0 \\ 0 \end{bmatrix}, \quad (23)$$

while choosing them along the z-axis implies that the vectors in Eq. 22 are rotated over the angle θ in the x-z plane, and

$$l_1 = \frac{\sqrt{s}}{2} \begin{pmatrix} 1 \\ \sin \theta \\ 0 \\ \cos \theta \end{pmatrix} = \sqrt{\frac{s}{2}} \begin{bmatrix} -t/s \\ -u/s \\ \sqrt{2tu}/s \\ 0 \end{bmatrix},$$

$$l_2 = \frac{\sqrt{s}}{2} \begin{pmatrix} 1 \\ -\sin \theta \\ 0 \\ -\cos \theta \end{pmatrix} = \sqrt{\frac{s}{2}} \begin{bmatrix} -u/s \\ -t/s \\ -\sqrt{2tu}/s \\ 0 \end{bmatrix}. \quad (24)$$

Rotating the lepton momenta is less cumbersome than rotating the hadron momenta in Eqs. 22.

For the jet momenta, which are just light-like directions, we have

$$k_1 = \frac{P_1}{\zeta_1} + p_{1\perp} - \frac{\mu_{1\perp}^2}{s} k_2, \quad (25)$$

$$k_2 = \frac{P_2}{\zeta_2} + p_{2\perp} - \frac{\mu_{2\perp}^2}{s} k_1. \quad (26)$$

We nicely have $\zeta_1 = P_1 \cdot k_2 / k_1 \cdot k_2$ and $\zeta_2 = P_2 \cdot k_1 / k_1 \cdot k_2$. The non-collinearity measures introduced in the previous section are

$$q_T = -p_{1\perp} - p_{2\perp} - \frac{\mu_{2\perp}^2}{s} k_1 - \frac{\mu_{1\perp}^2}{s} k_2, \quad (27)$$

$$\begin{aligned} q_T^2 &= (p_{1\perp} + p_{2\perp})^2 + \frac{\mu_{1\perp}^2 \mu_{2\perp}^2}{s} \\ &\approx (p_{1\perp} + p_{2\perp})^2 \end{aligned} \quad (28)$$

and with $p_{i\perp} = (p_{i\perp}^x, p_{i\perp}^y) = |p_{i\perp}|(\cos \varphi_i, \sin \varphi_i)$, we get

$$\begin{aligned} D_T &= -|p_{1\perp}| \sin \theta \sin \varphi_1 \left(1 - \frac{\mu_{2\perp}^2}{s}\right) \\ &\quad - |p_{2\perp}| \sin \theta \sin \varphi_2 \left(1 - \frac{\mu_{1\perp}^2}{s}\right) \\ &\quad - \frac{|p_{1\perp}| |p_{2\perp}|}{\sqrt{s}} \cos \theta \sin(\varphi_1 - \varphi_2) \\ &\approx -(p_{1\perp}^y + p_{2\perp}^y) \sin \theta + \frac{(p_{1\perp}^x p_{2\perp}^y - p_{1\perp}^y p_{2\perp}^x)}{\sqrt{s}} \cos \theta \\ &\approx q_T^y \sin \theta + \frac{\mathbf{p}_{1\perp}^{cm} \times \mathbf{p}_{2\perp}^{cm}}{\sqrt{s}} \cos \theta, \end{aligned} \quad (29)$$

where (illustrated in figure 1) the y -direction is the one orthogonal to the plane formed by the lepton and (back-to-back) jet directions. In Eq. 29 one recognises

$$\epsilon^{l_1 P_1 l_2 P_2} / \zeta_1 \zeta_2 \approx \epsilon^{l_1 l_2 k_1 p_{2\perp}} + \epsilon^{l_1 l_2 p_{1\perp} k_2} - \epsilon^{l_1 l_2 p_{1\perp} p_{2\perp}}, \quad (30)$$

following from Eqs. 25 and 26 omitting mass corrections. The third term in Eq. 30 corresponds to the $1/\sqrt{s}$ suppressed term in Eq. 29.

In this section, knowledge of all components of the hadrons in the (theoretical) lepton-parton CM frame has been assumed. The magnitude of the combined transverse-momentum components can be extracted from the lepton and hadron momenta in the lepton CM frame via the approximate relation in Eq. 28, but the azimuthal orientation of the hadrons cannot be determined as is clear from Eq. 29. It is only possible to obtain information on the azimuthal orientation in the lepton-parton CM frame if we know the partonic axis. The latter can be reasonably well approximated by the thrust axis. In order to study this, let us consider hadron 1 as the one to be studied, thus $1 \rightarrow h$ and identify hadron 2 with jet 2, $k_2 = P_2/\zeta_2$. In that case $M_2 = |p_{2\perp}| = 0$, the angle φ_2 becomes undefined and $\zeta_2 = 1$. We get the information on hadron 1 = h obviously from $q_T = -p_{h\perp} = -P_{h\perp}/\zeta_h$,

$$q_T^2 = -|p_{h\perp}|^2 \quad (31)$$

$$D_T = -|p_{h\perp}| \sin \theta \sin \varphi_h = q_T^y \sin \theta, \quad (32)$$

everything measured with respect to the jet direction.

IV. FEATURES IN DATA

In this section, observables discussed above are illustrated using a PYTHIA Monte-Carlo simulation [7] of the process $e^+e^- \rightarrow q\bar{q}$ at a CM energy of 10.58 GeV, where $q(\bar{q})$ represents an (anti-)up, down or strange quark. This energy corresponds to the $\Upsilon(4S)$ mass, and is characteristic for data collection at the Belle and BaBar experiments [8]. Quantum electrodynamics radiative effects are absent in the simulation, and hadron pairs are selected based on the value of their generated momentum. Unless stated otherwise, results are shown for pairs of positively charged pions.

In figure 3, left, the hadron momentum fractions ζ_1 (continuous, red line), ζ_1^{col} (large-dashed, blue line), and z_1 (dash-dotted, green line) are presented for hadrons that lie in the hemisphere opposite to that of the second hadron in the event. In order to fulfil the latter condition, only hadron pairs with negative three-momentum scalar product are considered. As can be seen from the figure, the variables ζ_1^{col} and z_1 are contained in the interval between 0 and 1¹, while the value of ζ_1 exceeds 1. If the variable ζ_2 of the second hadron is required to be not too small, not smaller than 0.05 in the present case, then ζ_1 is also constrained to $0 \leq \zeta_1 \leq 1$, as illustrated by the short-dashed, orange curve, and it follows the distribution of ζ_1^{col} .

When selecting hadrons that lie in the same hemisphere, as shown in figure 3, right, a larger amount of hadrons have a momentum fraction ζ_1 larger than 1 (continuous, red line). In addition, also negative values for ζ_1 are now observed. Requiring again $\zeta_2 > 0.05$, restricts ζ_1 to $0.0 \leq \zeta_1 \leq 0.5$ (short-dashed, orange line). Also ζ_1^{col} is confined to this interval, while z_1 lies as before between 0 and 1. Hadrons originating from the same quark need to share half of the available CM energy. This is reflected in the upper limit of 0.5 for ζ_1 and ζ_1^{col} .

If the hemisphere selection of hadrons is not based on their relative orientation, but on their orientation with respect to the thrust axis, a small fraction of hadrons have a negative ζ_1 value when considering the configuration of opposite hemispheres, as can be seen in figure 4 (continuous, red line). These hadrons correspond to pairs that are associated to the same hemisphere when basing the selection criterion on the hadrons' relative orientation. Requiring $\zeta_2 > 0.05$ removes these hadrons from the selection (short-dashed, orange line).

For low-energetic hadrons there is an ambiguity in the determination of hemispheres, while for hadrons with fractional momenta above 0.1 both hemisphere selection criteria coincide, as can be seen from the comparison of open and closed symbols for ζ_1 , ζ_1^{col} , and z_1 in figure 5. Most commonly, experimental measurements are

¹ In the limit of massless hadrons or infinite CM energy, the values 0 and 1 would effectively be reached.

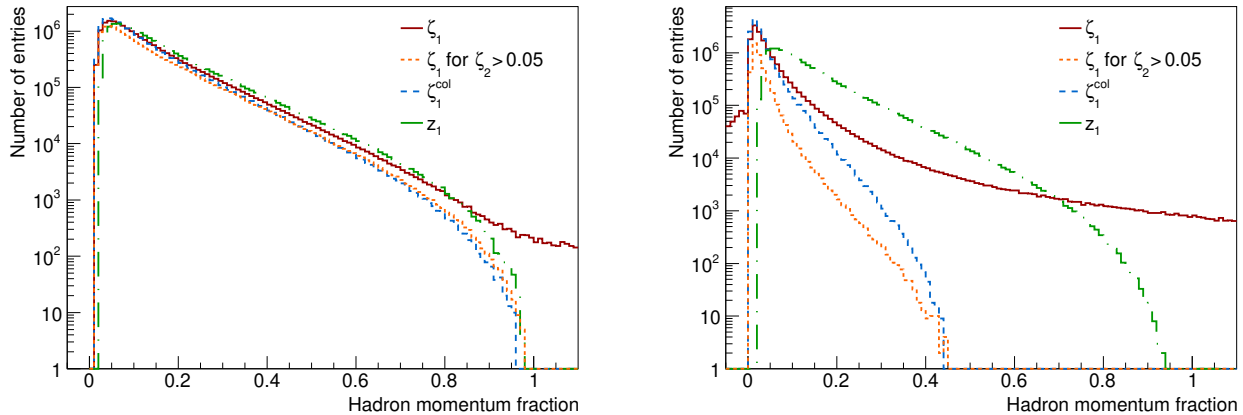


FIG. 3: Hadron momentum fractions ζ_1 (continuous, red line), ζ_1 for $\zeta_2 > 0.05$ (short-dashed, orange line), ζ_1^{col} (large-dashed, blue line), and z_1 (dash-dotted, green line) for hadrons in the opposite (left) and same (right) hemisphere, based on their relative orientation.

restricted to fractional hadron momenta above 0.1 because of instrumental limitations, while phenomenological extractions of fragmentation functions from experimental data avoid low- z regions because of singularities in the QCD evolution equations [9]. Figure 5 also makes clear that at small values of fractional momentum, the three variables ζ , ζ^{col} , and z are relatively close to each other, with a good agreement between ζ and ζ^{col} , while at larger values, they differ more.

Alternatively, the difference between ζ and z is also visible in figure 6. In this figure, $\sqrt{-q_T^2}$ is presented (dashed, blue line) together with $|P_{2t}|/\zeta_2$ (continuous,

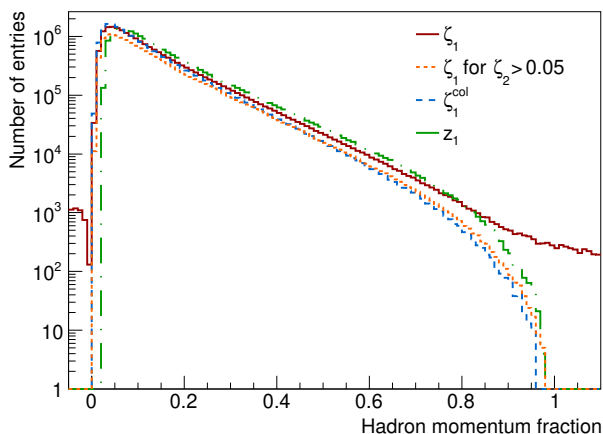


FIG. 4: Hadron momentum fractions ζ_1 (continuous, red line), ζ_1 for $\zeta_2 > 0.05$ (short-dashed, orange line), ζ_1^{col} (large-dashed, blue line), and z_1 (dash-dotted, green line) for hadrons in opposite hemispheres, based on their orientation with respect to the thrust axis.

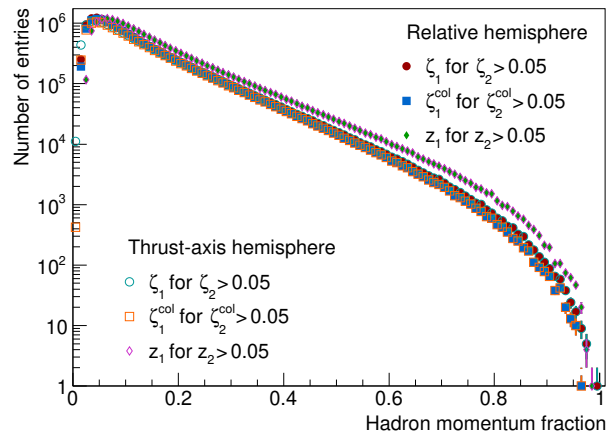


FIG. 5: Hadron momentum fractions ζ_1 for $\zeta_2 > 0.05$ (circles), ζ_1^{col} for $\zeta_2^{col} > 0.05$ (squares), and z_1 for $z_2 > 0.05$ (diamonds) for hadrons in opposite hemispheres based on their relative orientation (filled symbols) and based on their orientation with respect to the thrust axis (open symbols). The vertical error bars represent the square root of the number of entries in each bin.

red line) and $|P_{2t}|/z_2$ (dash-dotted, green line). Here, P_{2t} refers to the component of hadron 2 orthogonal to P_1 of hadron 1, all measured in the CM frame and with hadron 1 and hadron 2 required to lie in opposite hemispheres. The results are shown for $\zeta_1 = \zeta_2$ comprised between 0.15 and 0.20 (left) and between 0.40 and 0.50 (right). While $\sqrt{-q_T^2}$ and $|P_{2t}|/\zeta_2$ (as expected from Eq. 1) agree, up to mass corrections, over the full range, both for low and higher regions of hadron fractional momentum, $|P_{2t}|/z_2$ only agrees with them at low values of $|P_{2t}|/\zeta_2$, strongly differing at higher values. This also illustrates the ap-

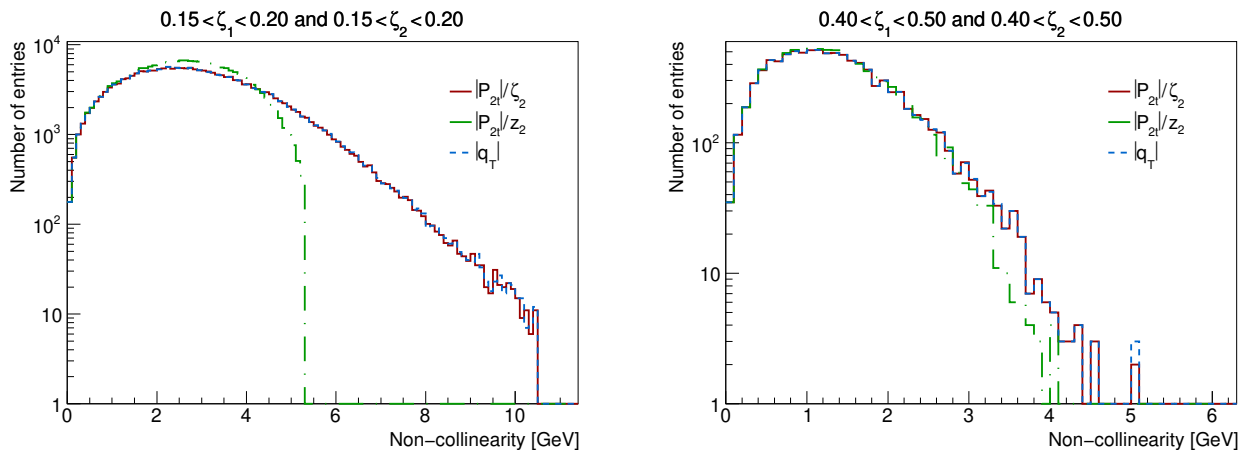


FIG. 6: The non-collinearity variables $\sqrt{-q_T^2}$ (dashed, blue line), $|P_{2t}|/\zeta_2$ (continuous, red line), and $|P_{2t}|/z_2$ (dash-dotted, green line) for $0.15 < \zeta_1 = \zeta_2 < 0.20$ (left) and $0.40 < \zeta_1 = \zeta_2 < 0.50$ (right) for hadrons in opposite hemispheres.

proximate relation in Eq. 16, which shows that the difference between ζ and z increases with increasing $|q_T|$. In addition we note that the variable $|P_{2t}|/z_2$ is restricted to an upper limit of $\approx \sqrt{s}/2$.

In figure 7, the distributions of ζ_2^{col} versus ζ_1^{col} (left) and z_2 versus z_1 (right) are presented for three ranges in R_{12} : $0.00600 < R_{12} < 0.00625$, $0.02500 < R_{12} < 0.03000$, and $0.19750 < R_{12} < 0.20250$. The respective hemisphere orientation of the hadrons and the sign of ζ_i are identified by different colours. For the two highest intervals in R_{12} , the lower limit of the interval is also indicated in the figures (vertical and horizontal lines). The value of R_{12} determines the minimal values that z_i and ζ_i^{col} can take, as follows from Eqs. 9 and 13. The diagonal lines correspond to $\mathbf{v}_1 \cdot \mathbf{v}_2 = -1$ or $\mathbf{v}_1 \cdot \mathbf{v}_2 = 0$, as indicated. The latter delimits the configurations where the hadron pairs have the same or the opposite orientation for the respective values of R_{12} . When $\mathbf{v}_1 \cdot \mathbf{v}_2 = -1$, $\zeta_1^{col} \zeta_2^{col}$ attains its maximum, while $z_1 z_2$ reaches its minimum. These products $\zeta_1^{col} \zeta_2^{col}$ and $z_1 z_2$ are then equal to R_{12} .

For low enough values of R_{12} and for hadrons in the same hemisphere, ζ_i can be negative. These events are indicated in red. The boundary line for points with $\zeta_i < 0$ follows from Eq. 2 or 14. The numerator of Eq. 14 for ζ_1 is always positive, but the denominator turns negative if $\zeta_2^{col}/\zeta_1^{col} < 2M_K^2/R_{12}s$. This effect is more clearly visible in figure 8, where the distribution for a kaon-pion pair is presented and then particularly the region of $\zeta_K < 0$ for smallest $R_{12} \approx 0.006$, in which case the relation is $\zeta_K^{col}/\zeta_\pi^{col} = 2M_K^2/R_{12}s \approx 0.7$. It is asymmetric as for the same R_{12} we have for pions $\zeta_\pi^{col}/\zeta_K^{col} = 2M_\pi^2/R_{12}s \approx 0.06$. Note also that the larger kaon mass creates a distortion of the distributions. The effect is more prominent for the lowest value of R_{12} . This region of R_{12} is actually lower than the ‘safe region’ $R_{12} \sim 1 \text{ GeV}^2/s$. The analogous situation occurs

for the z_i distribution.

For the here presented highest region in R_{12} , there are only hadrons originating from opposite hemispheres. One has from Eq. 9 that for the same-hemisphere configuration, $z_1 z_2$ is at its minimum for $\mathbf{v}_1 \cdot \mathbf{v}_2 = 0$. In this limit, and with $R_{12} = 0.2$, one obtains $z_1 z_2 = 0.4$. For this value of $z_1 z_2$, $z_1 + z_2 > 1$. Hence hadron pairs cannot originate from the same hemisphere, as indeed is observed from figures 7 and 8. For values of $R_{12} > 0.125$, there are no hadron pairs in the same hemisphere, as follows from Eq. 9.

Equations 9 and 11 are illustrated in figure 9, where $R_{12}s/(2z_1 z_2)$ is shown for increasing ranges of $z_1 = z_2$ for hadron pairs irrespective of their hemisphere (continuous, blue line) and for hadron pairs in opposite hemispheres (dashed, red line). At $z_1 z_2 = 2R_{12}$, i.e., $R_{12}s/(2z_1 z_2) = s/4 = 27.98 \text{ GeV}^2$, there is a sharp separation between the regions corresponding to the same-hemisphere and opposite-hemisphere configuration. At low values of fractional momenta, the transition between these regions is continuous, while for higher fractional momenta, both regions are progressively better separated from each other. With increasing fractional momenta, there are also gradually less pairs of hadrons belonging to the same hemisphere, while at the highest values of z_i , their contribution completely disappears.

In figure 10, $|p_{h\perp}|$ obtained from Eq. 31 (open, red circles), using the thrust axis as reference axis, is compared to the hadron transverse-momentum component with respect to the $q\bar{q}$ axis scaled with ζ_h , $p_{h\perp}^{q\bar{q}}$ (filled, blue squares), for $0.15 < \zeta_h < 0.20$ (left) and $0.40 < \zeta_h < 0.50$ (right). A lower limit on the value of the thrust variable of 0.85 is required in order to select events that have a two-jet configuration. This cut affects the distribution of the transverse momentum, since it affects to which degree tracks are collimated rather than isotropically distributed. At small values of $|p_{h\perp}|$, there is good

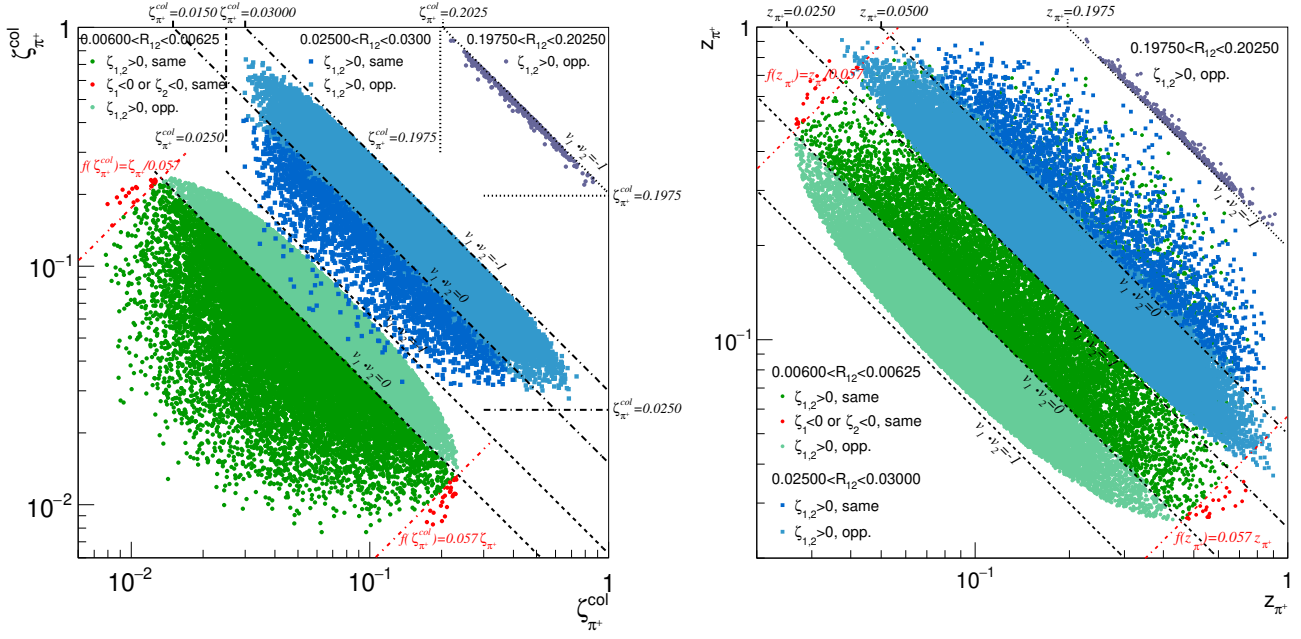


FIG. 7: Distributions of ζ_2^{col} versus ζ_1^{col} (left) and of z_2 versus z_1 (right) for three ranges in R_{12} : $0.00600 < R_{12} < 0.00625$, $0.02500 < R_{12} < 0.03000$, and $0.19750 < R_{12} < 0.20250$. The hemisphere configuration and the sign of ζ_i are indicated in the figure. The diagonal lines indicate the limit for which $v_1 \cdot v_2$ is equal to 0 or -1 . The vertical and horizontal lines correspond to the lower limit of the respective R_{12} intervals.

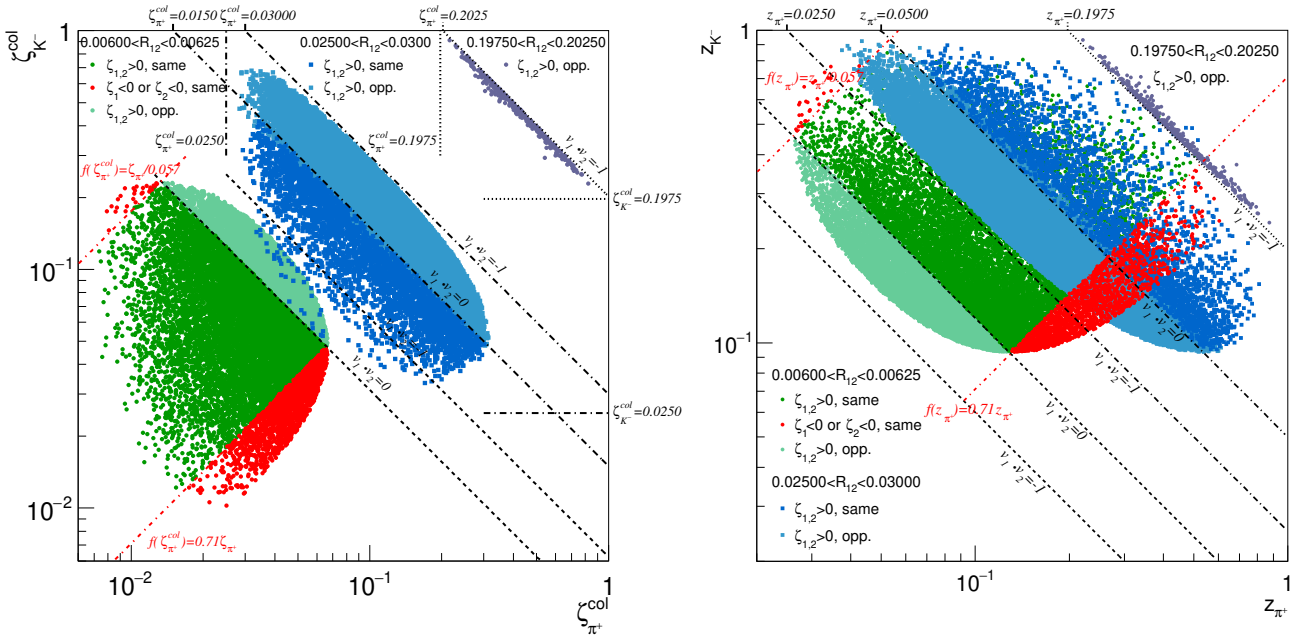


FIG. 8: As for figure 7, but for an oppositely charged kaon-pion pair.

agreement between the generated distribution and that obtained from Eq. 31. At larger values disagreement is observed, which can be explained by the contribution of events where more than two jets are created.

In figure 11, $\sin \varphi_h$ extracted from Eq. 32 (open, red

circles), using the thrust axis as reference, with as explained for Eqs. 31 and 32, ζ of the thrust axis set to 1 and the magnitude of the thrust axis normalised to $\sqrt{s}/2$, is compared to $\sin \varphi_h^{q\bar{q}}$, where the angle $\varphi_h^{q\bar{q}}$ is the angle between the plane containing the $q\bar{q}$ axis and the e^+e^-

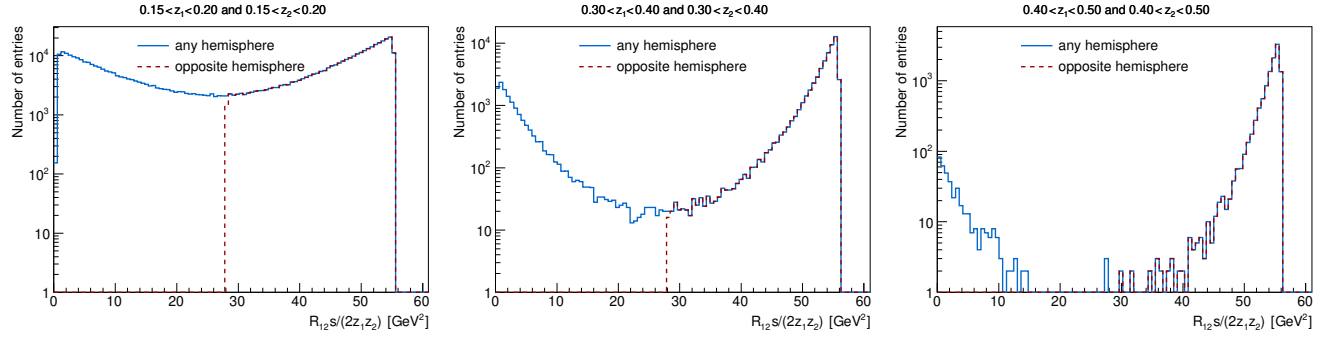


FIG. 9: The quantity $R_{12}s/(2z_1 z_2)$ for $0.15 < z_1 = z_2 < 0.20$ (left), $0.30 < z_1 = z_2 < 0.40$ (middle), and $0.40 < z_1 = z_2 < 0.50$ (right) for hadrons irrespective of their hemisphere (continuous, blue line), and for hadrons in opposite hemispheres (dashed, red line).

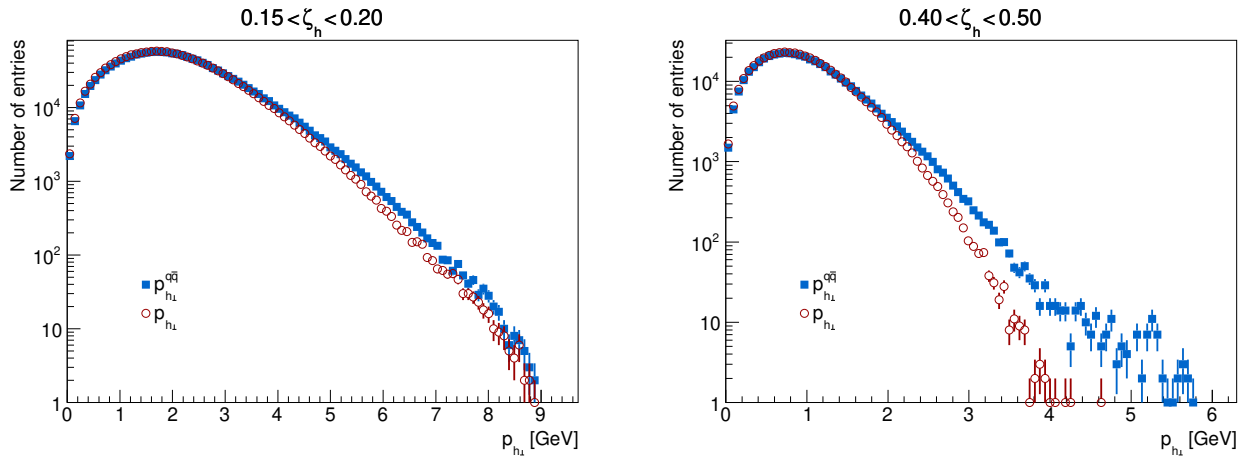


FIG. 10: The scaled transverse momentum $p_{h\perp}$ extracted from q_T (red, open circles), using the thrust axis as reference, and the transverse momentum of hadron h with respect to the $q\bar{q}$ axis, scaled with ζ_h (blue, closed squares) for $0.15 < \zeta_h < 0.20$ (left) and $0.40 < \zeta_h < 0.50$ (right).

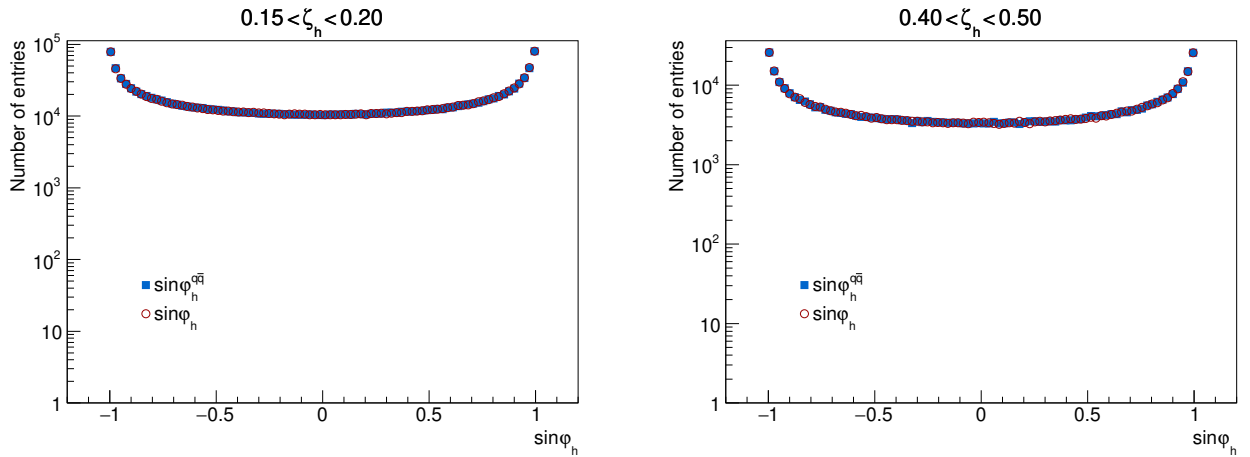


FIG. 11: The quantity $\sin \varphi_h$ extracted from D_T (red, open circles), using the thrust axis as reference, and $\sin \varphi_h^{q\bar{q}}$ of hadron h with respect to the plane formed by the lepton and $q\bar{q}$ axis (blue, closed squares) for $0.15 < \zeta_h < 0.20$ (left) and $0.40 < \zeta_h < 0.50$ (right).

axis and the plane containing the $q\bar{q}$ axis and hadron h . The ζ_h ranges covered are the same as those in figure 10 and also here a minimal thrust value of 0.85 is required. The distribution is insensitive to the latter requirement. The $\sin\varphi_h$ and $\sin\varphi_h^{q\bar{q}}$ distributions show a very good agreement, irrespective of the value of ζ_h . Extracting the determinant defined in Eq. 17, using as reference the thrust axis, offers thus the possibility to learn about the hadron azimuthal distribution.

To illustrate the D_T distribution by itself, we begin by recalling that it is not uniformly distributed in θ . Firstly, the θ -dependence is determined by the hard process, where we expect the cross section of $e^+e^- \rightarrow q\bar{q}$ to have a $(1 + \cos^2\theta)$ behavior. This dependence, ideally, is decoupled from the non-collinearity due to the fragmentation process. Secondly, there is the $\sin\theta$ and $\cos\theta$ dependence that comes back in the orientation of the hadron production planes as defined in figure 1 and appears in Eq. 29. In particular close to $\theta = 0$ and $\theta = \pi$, there is a contribution of the second term in Eq. 29, even if its magnitude is suppressed by a factor $|p_\perp|/\sqrt{s} \lesssim 0.1$ as compared to the first term. Note, however, that for $\theta = 0$ and $\theta = \pi$, the azimuthal angle is not defined. In figure 12, the distribution of $D_T/\sin\theta$ is shown for two hadrons from opposite hemispheres (left) and for the configuration of a hadron and the thrust axis (right). Here,

$$\sin\theta = \frac{2\sqrt{tu}}{s} = \frac{4\sqrt{(l_1 \cdot k_1)(l_2 \cdot k_1)}}{s} \quad (33)$$

is obtained from the directions in the CM frame of the lepton axis and a (fast) hadron or the thrust axis:

$$\sin\theta \approx \frac{|l_1 \times P_1|}{|l_1||P_1|}, \quad (34)$$

where P_1 is to be replaced by P_{thrust} when considering the thrust axis. Other possible approximations for $\sin\theta$, in order of decreasing accuracy, involve one or two of the hadron momenta,

$$\sin\theta \approx \frac{4\sqrt{(l_1 \cdot P_1)(l_2 \cdot P_1)}}{\zeta_1 s} \quad (35)$$

$$\approx \frac{4\sqrt{(l_1 \cdot P_1)(l_1 \cdot P_2)}}{s\sqrt{\zeta_1\zeta_2}}, \quad (36)$$

where the hadron P_1 in the first equation or one of the hadrons in the second equation can be replaced by P_{thrust} (and also ζ_{thrust}), which gives a better accuracy. In particular, replacing the hadron in the first approximation by the thrust axis coincides with Eq. 34 for the thrust axis. The $D_T/\sin\theta$ distribution shows a dependence on θ for low and mid values of θ , whereas for higher values, where the $\cos\theta$ contribution in D_T is strongly suppressed, no θ dependence is observed. The distribution from two opposite hemisphere hadrons nicely shows a transverse momentum distribution with a width of the order of 1.5 GeV. Using the thrust axis and one hadron the width is about 1.0 GeV, indeed something like a factor $1/\sqrt{2}$ less

as expected for a uniform transverse momentum distribution.

V. CONCLUSIONS

Two measures for non-collinearity have been introduced and discussed. One is the invariant length of the non-collinearity vector q_T , in a back-to-back jet situation directly related to the transverse momenta of partons in the hadrons that are produced in the hadronisation process. The other is a determinant constructed from the two lepton momenta and the hadron and thrust momenta, or from the two lepton momenta and two opposite-hemisphere-hadron momenta, which in the back-to-back jet situation contains information on the transverse momentum orthogonal to the lepton-parton plane. The latter thus also contains information on the azimuthal orientation of the back-to-back partons through the orientation of the momenta of the produced hadrons with respect to the lepton plane.

Our results show that the 2PI variables (ζ) are perfectly suitable to correct for various shortcomings of the variables ζ^{col} or the CM energy fractions z . The 2PI variables ζ by construction account for hadronic mass corrections and the deviation from non-collinearity. They are not constrained between 0 and 1 as the other variables, but in the back-to-back jet situation the ζ 's also tend to approximate light-cone momentum fractions (just as ζ^{col}), which are suitable variables when it comes to QCD factorisation.

In how far the given measures for non-collinearity, q_T and D_T , measure the transverse momenta for an individual fragmenting parton depends on the appropriate definition of these quantities in a high energy scattering process. We considered in this note their importance as approximants of quantities that have a natural interpretation in the back-to-back two-jet situation.

All quantities and corresponding distributions have been exemplified with studies from a Monte-Carlo simulation. Alongside, three different momentum fractions have been presented and compared, and their relation to quantities characterising hemisphere orientation and the transverse momentum acquired in the hadronisation process has been exposed.

Acknowledgements

We acknowledge useful discussions with several colleagues, among them Daniël Boer, Alessandro Bacchetta and Marco Radici. We are grateful to Ralf Seidl for the Monte-Carlo simulation. PJM acknowledges the support of the FP7 EU "Ideas" programme QWORK (Contract 320389). CVH acknowledges the support from the Basque Government (Grant No. IT956-16) and the Ministry of Economy and Competitiveness (MINECO) (Juan de la Cierva), Spain.

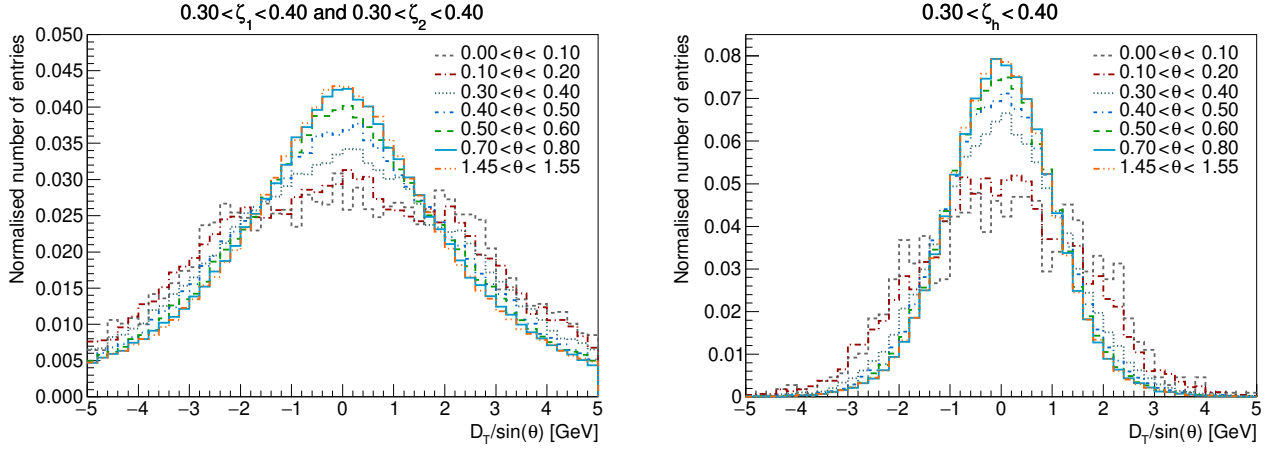


FIG. 12: The distribution of $D_T/\sin\theta$ for the event configuration considering pairs of hadrons from opposite hemispheres (left) and the hadron–thrust-axis combination (right), for $0.3 < \zeta_{1,2(h)} < 0.4$ and for different ranges of $\sin\theta$, as indicated.

-
- [1] J.P. Ralston and D.E. Soper, Nucl. Phys. B **152** (1979) 109.
- [2] J.C. Collins and D.E. Soper, Nucl. Phys. B **193** (1981) 381 [Erratum: Nucl. Phys. B **213** (1983) 545].
- [3] J.C. Collins and D.E. Soper, Nucl. Phys. B **194** (1982) 445.
- [4] D. Boer, R. Jakob and P.J. Mulders, Nucl. Phys. B **504** (1997) 345-380.
- [5] G. Altarelli, R.K. Ellis, G. Martinelli and So-Young Pi, Nucl. Phys. B **160** (1979) 301-329.
- [6] R. P. Feynman, Photon-hadron interactions (Benjamin, Reading, MA, 1972).
- [7] T. Sjöstrand et al., Comp. Phys. Commun. **135** (2001) 238-259.
- [8] A. J. Bevan et al., Eur. Phys. J. C **74** (2014) 3026.
- [9] D. de Florian, R. Sassot, and M. Stratmann, Phys. Rev. D **75** (2007) 114010.